A systematic framework to construct unconventional superconducting pairing scar states using multi-body interactions

Shohei Imai[1] and Naoto Tsuji[1, 2]

[1]*Department of Physics, University of Tokyo, Hongo, Tokyo 113-0033, Japan*
[2]*RIKEN Center for Emergent Matter Science (CEMS), Wako 351-0198, Japan*
(Dated: April 5, 2024)

We present a systematic framework to construct model Hamiltonians that have unconventional superconducting pairing states as exact energy eigenstates, by incorporating multi-body interactions (i.e., interactions among more than two particles). The multi-body interactions are introduced in a form of the local density-density coupling in such a way that any pair configuration in real space has the same interaction energy by cancelling the two-body and multi-body interactions. Our approach is applicable to both spinless and spinful models in any spatial dimensions and on any bipartite lattices, facilitating an exhaustive extension of Yang's s-wave η-pairing state to various other unconventional pairing symmetries (p-wave, d-wave, f-wave, etc.). We verify that the two-dimensional spinful Hubbard model on a square lattice with the multi-body interactions has the d-wave pairing state as an energy eigenstate, which can be regarded as a quantum many-body scar state as evidenced from the numerical analysis of the pair correlation function, the entanglement entropy, and the level statistics. We also discuss other examples, including f-wave pairing states on a honeycomb lattice, s-wave pairing states in a nearest-neighbor interacting system, and spinless p-wave pairing states in one dimension.

I. INTRODUCTION

Out-of-equilibrium superconductivity offers a potential to realize exotic quantum many-body states that are otherwise impossible to be found in thermal equilibrium. Notable candidates for those states include photoinduced superconducting-like states that have been experimentally observed even above the equilibrium transition temperature [1–5] (see also [6, 7]). Another example is the Floquet engineering [8–10] (i.e., quantum states induced by a time-periodic drive), which has endowed superconductors with topological properties [11–16]. A variety of transient drives have also been employed to induce superconductivity with unconventional pairing states—such as bulk odd-frequency pairings [17, 18] and finite-momentum pairing states [19, 20]—which are challenging to be realized in equilibrium.

Although numerous intriguing experiments and theoretical proposals have been proposed, the problem is how such a non-thermal state can be made robust against thermalization. To generate nonequilibrium states, one necessarily injects a finite amount of energy to the system, which turns into heat in a general quantum many-body system. This results in the suppression (or vanishing) of superconducting correlations within a finite timescale. In order to overcome this difficulty, it is crucial to seek for a certain mechanism that protects nonequilibrium superconducting states from thermalization even in the presence of many-body interactions.

As a promising mechanism to maintain superconducting correlations for a sufficiently long time at highly excited states, there have been proposed quantum many-body scar (QMBS) states [21–23], which are exceptional energy eigenstates that do not have thermal properties in a nonintegrable system. According to the eigenstate thermalization hypothesis (ETH) [24–27], all excited energy eigenstates in a nonintegrable model are expected to be indistinguishable from thermal states as long as one refers to few-body observables. QMBS states are considered to be an exception to the ETH, as characterized by long-

lived nonthermal dynamics in nonintegrable systems [28–48]. Several methods to construct a model Hamiltonian that accommodates a target state as a QMBS state have been proposed, such as the (restricted) spectrum-generating algebra [30], the embedding formalism [22], and the symmetry-based formalism [49].

A primary example of a nonthermal energy eigenstate in a nonintegrable system that supports superconducting correlations is the so-called η-pairing state, which is an exact energy eigenstate of the Hubbard model on a d-dimensional square lattice, as shown by C. N. Yang [50]. Yang's η-pairing state corresponds to a condensate of doublons carrying finite momentum, and exhibits long-range superconducting correlations with the s-wave pairing symmetry. If one classifies the Hilbert space in terms of symmetry sectors, the η-pairing state is the only eigenstate in the corresponding sector [51, 52]. In this respect, strictly speaking, the η-pairing state is not considered to be a QMBS state, while there have been several proposals to modify the Hamiltonian to make it a true QMBS state [49, 53–59]. Similar η-pairing states have been recently proposed to be realized by photo-irradiation [19], and have attracted interest as a mechanism to induce superconductivity by light.

In this paper, we generalize Yang's η-pairing state to those with various unconventional pairing symmetries (p-wave, d-wave, f-wave, etc.), and establish a systematic framework to construct model Hamiltonians that have the unconventional pairing states as QMBS states. This will open up a way to realize a family of unconventional superconducting nonthermal states with Cooper pairs having finite momentum, most of which are difficult to be accessed in equilibrium conditions. In particular, given the known instability of Yang's η-pairing state to perturbations, such as due to the long-range Coulomb interaction and the coupling to electromagnetic fields [60, 61], it will be important to explore possible pairing states with different symmetries, which may offer an opportunity to stabilize those states against perturbations. Recent studies have extended Yang's η-pairing state to encompass spinless
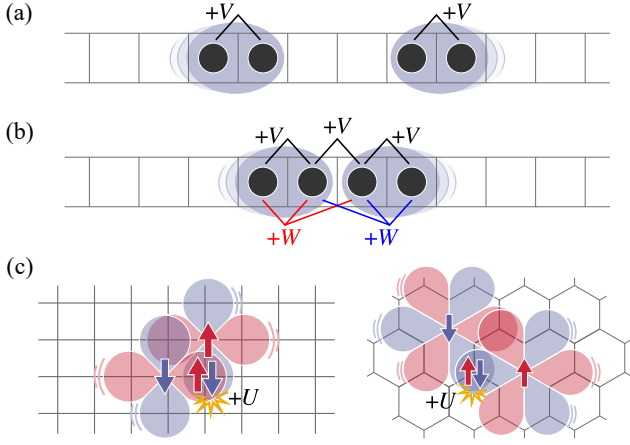
FIG. 1. (a), (b) Examples of spatial configurations of the p-wave pairing state in a one-dimensional spinless fermion model. (a) When two pairs (blue clouds) are separated to each other, the two-body interaction V only acts within each pair. (b) When two pairs come next to each other, there is an additional energy increment V, which can be cancelled by the three-body interaction W (if one chooses $V + 2W = 0$). (c) Schematic picture of unconventional superconducting pairs of spinful fermions with d-wave (left panel) and f-wave (right) pairing symmetries (indicated by blue and red clouds) on the square and honeycomb lattices, respectively. Two pairs feel an energy cost U due to the two-body interaction when they overlap with each other.

fermions [62, 63] and multi-component systems [58, 64–67].

If one naively extends the η-pairing states to those with other pairing symmetries, (e.g., for p-wave pairing states in one dimension, see Fig. 1(a)), one can still see that they are eigenstates of the kinetic term in a Hubbard model (see below for more details), in much the same way as in the case of Yang's η-pairing state [50]. The real challenge is in the interaction term: When two off-site pairs come close to each other, they feel an additional energy cost due to the two-body interaction. This prevents the unconventional pairing states from being eigenstates of the interaction term (and hence the total Hamiltonian) in the Hubbard model.

To overcome this difficulty, we engineer multi-body interactions (i.e., interactions among more than two particles) to cancel the energy increment of pairs due to the two-body interaction. For example, in a one-dimensional spinless fermion model we can introduce a three-body interaction to cancel the nearest-neighbor two-body interaction acting on the pairs (Fig. 1(b)). The cancellation works for arbitrary pair configurations, no matter how many pairs are distributed on the lattice. In this way, the p-wave pairing state can be made an exact eigenstate of the one-dimensional Hubbard model with the three-body interaction. Previously, it has been proposed that the p-wave pairing state becomes an exact eigenstate in a model with the three-body interaction and/or density-dependent hopping [62, 63], but our construction only requires the three-body interaction.

The advantage of our approach is that it can be systematically generalized to other pairing symmetries including spin degrees of freedom in higher dimensions (see Fig. 1(c)). To this end, we introduce an extended number operator [$\mathbb{n}_{i\sigma}$ in Eq. (17)]

that signals whether spin-σ particles exist or not on lattice sites next to i site. Using this operator, we can systematically cancel the interaction energy between off-site pairs, and obtain a model Hamiltonian with multi-body interactions that has unconventional pairing states as exact eigenstates. We note that the derived interaction is strictly local, and takes a form of the density-density coupling between M particles ($M \leq M_{max}$ with M_{max} being finite and system-size independent).

We apply the framework to the spinful Hubbard model with multi-body interactions on the two-dimensional square lattice, and show that the model has an exact eigenstate with the d-wave pairing symmetry (the left panel of Fig. 1(c)). We numerically evidence that the model is nonintegrable from the analysis of energy level statistics. We also find that the d-wave pairing state shows the subvolume law of entanglement entropy and the off-diagonal long-range order of superconductivity, which indicates that the d-wave pairing state is indeed a QMBS state. Other examples are also discussed, including f-wave pairing states on a honeycomb lattice (the right panel of Fig. 1(c)), s-wave pairing states in a nearest-neighbor interacting system, and spinless p-wave pairing states in one dimension.

The rest of this paper is organized as follows. In Sec. II, we introduce off-site η-pairing states, and demonstrate the idea of cancelling two-body interactions with multi-body ones to make the off-site η-pairing states eigenstates of a Hamiltonian. We will mainly focus on the case of the d-wave pairing symmetry on the two-dimensional square lattice as an example for explanation. We show that the unconventional η-pairing states become energy eigenstates of the multi-body interacting model. We numerically confirm that the unconvntional η-pairing states are quantum many-body scar states based on the analysis of the pair correlation function, entanglement entropy (Sec. III), and the level-spacing statistics (Sec. IV). We will discuss generalizations to other pairing symmetries and other lattice structures in Sec. V. Finally, we close the paper with the discussion (Sec. VI) and summary (Sec. VII) of this work.

Throughout the paper, we set the Dirac constant $\hbar = 1$ and the lattice constant $a = 1$.

II. SUPERCONDUCTING ENERGY EIGENSTATES WITH UNCONVENTIONAL PAIRING SYMMETRY

In this section, we present a systematic construction of model Hamiltonians that have unconventional pairing states as exact eigenstates.

In Sec. II A, we take a glance at the simplest case of the p-wave pairing state in a one-dimensional spinless fermion model, which contains the essence of our idea utilizing multi-body interactions to construct the model Hamiltonians. We then discuss how the model construction can be generalized to other pairing symmetries. Here, we focus on a two-dimensional spinful model with multi-body interactions on the square lattice. In Sec. II B, we define unconventional pairing states with off-site η-pairing operators, which are straightforward generalization of the s- and p-wave cases. In Sec. II C, we

see that the unconventional pairing states are not eigenstates of the two-body interacting model. In Sec. II D, we introduce an extended number operator, which measures whether neighboring sites are occupied by particles. Using this operator, we can exactly and systematically cancel the energy increment between off-site pairs coming from the two-body interaction. We show that the d-wave pairing state becomes an exact eigenstate of the multi-body interacting model.

A. p-wave pairing state in a one-dimensional spinless fermion system

Let us consider a one-dimensional spinless fermion model. Based on the analogy of Kitaev's spinless fermion model of p-wave topological superconductors [68], one can define a p-wave η-pairing operator and a p-wave η-pairing state [62, 63],

$$\eta_p^+ = \sum_j (-1)^j c_j^\dagger c_{j+1}^\dagger, \tag{1}$$

$$|\Psi_p^N\rangle = \frac{1}{\mathcal{N}_p^N} (\eta_p^+)^{N/2} |0\rangle, \tag{2}$$

respectively. Here, $c_i^\dagger$ (c_i) is the creation (annihilation) operator for spinless fermions at site i, N is the number of fermions (N is assumed to be even), $\mathcal{N}_p^N$ is the normalization constant (such that $\langle \Psi_p^N | \Psi_p^N \rangle = 1$), and $|0\rangle$ is the vacuum state. The operator η_p^+ creates an off-site pair with the p-wave pairing symmetry and the center-of-mass momentum π. The p-wave η-pairing state shows an off-diagonal long-range order with the p-wave pairing symmetry, which can be exactly evaluated [63]. One can see that these definitions are straightforward generalization of the Yang's s-wave η-pairing operator $\eta^+ = \sum_j (-1)^j c_{j\uparrow}^\dagger c_{j\downarrow}^\dagger$ ($c_{j\sigma}$ creates a fermion at site j with spin $\sigma = \uparrow, \downarrow$) and the Yang's s-wave η-pairing state $|\Psi^N\rangle \propto (\eta^+)^{N/2} |0\rangle$ in a spinful model [50] (see also Sec. V C). In Fig. 1(a) and (b), we illustrate examples of spatial configurations (Fock states in the coordinate basis) of the p-wave η-pairing state for $N/2 = 2$.

The Hamiltonian of the spinless Hubbard model that we consider here is given by $\mathcal{H} = \mathcal{H}_t + \mathcal{H}_V$ with

$$\mathcal{H}_t = -t \sum_i \left(c_i^\dagger c_{i+1} + \text{H.c.} \right), \tag{3}$$

$$\mathcal{H}_V = V \sum_i n_i n_{i+1}, \tag{4}$$

where $n_i = c_i^\dagger c_i$ is the number operator. The first term $\mathcal{H}_t$ (Eq. (3)) describes the nearest-neighbor particle hopping, and the second one $\mathcal{H}_V$ (Eq. (4)) represents the nearest-neighbor two-body interaction with an interaction strength V. For the kinetic term $\mathcal{H}_t$ (Eq. (3)), the p-wave η-pairing operator (Eq. (1)) satisfies the commutation relation $[\mathcal{H}_t, \eta_p^+] = 0$ for both the periodic and open boundary conditions. However, the p-wave η-pairing state is not an eigenstate of the interaction term (Eq. (4)), since adjacent pairs have an additional energy cost V, as displayed in Fig. 1(b).

To cancel the energy increment arising from the two-body interaction, we introduce the three-body interaction,

$$\mathcal{H}_W = W \sum_i n_i n_{i+1} n_{i+2}, \tag{5}$$

with the interaction strength W. We observe that when two pairs come next to each other there always appear two combinations of neighboring three particles (Fig. 1(b)). This motivates us to choose the three-body interaction parameter $W = -V/2$, which cancels the energy increase due to the two-body interaction. The cancellation works for arbitrary number $N/2$ of pairs no matter how they distribute on the lattice. Hence, the p-wave η-pairing state becomes an exact eigenstate of the Hubbard model with the three-body interaction (with $W = -V/2$),

$$\mathcal{H} = \mathcal{H}_t + \mathcal{H}_V + \mathcal{H}_W, \tag{6}$$

$$\mathcal{H}|\Psi_p^N\rangle = \frac{N}{2} V |\Psi_p^N\rangle, \tag{7}$$

with the eigenenergy $NV/2$ (coming from the nearest-neighbor two-body interaction within each pair). Let us remark that the derived interaction part of the Hamiltonian takes a form of

$$\mathcal{H}_V + \mathcal{H}_W = V \sum_i n_i n_{i+1} \left(1 - \frac{1}{2} n_{i+2} \right), \tag{8}$$

which suggests a hint for generalization to other pairing symmetries in higher dimensions.

B. Off-site η-pairing operators and d-wave pairing states

Having established the p-wave η-pairing state as an exact eigenstate of the three-body interacting system in the previous subsection, we discuss how the model construction can be generalized to other pairing symmetry cases including spin degrees of freedom in higher dimensions.

Let us define an off-site η-pairing creation operator in two dimensions as

$$\eta_\alpha^+ = \sum_i e^{i\boldsymbol{\pi}\cdot\boldsymbol{r}_i} c_{\boldsymbol{r}_i,\uparrow}^\dagger c_{\boldsymbol{r}_i+\boldsymbol{\alpha},\downarrow}^\dagger, \tag{9}$$

where $\boldsymbol{\alpha}$ represents a separation between two particles in a pair, the site index i runs over the entire lattice sites, $\boldsymbol{\pi} = (\pi, \pi)$ is the center-of-mass crystal momentum of pairs, and $c_{\boldsymbol{r}_i,\sigma}$ is the fermion annihilation operator with spin σ ($=\uparrow, \downarrow$) at position $\boldsymbol{r}_i$. This definition is the same as Eq. (26) in Ref. [50].

Here we focus on the case of nearest-neighbor pairs on the square lattice, in which we can take four independent η-pairing operators $\eta_{\pm e_x}^+$ and $\eta_{\pm e_y}^+$ with $\boldsymbol{e}_x = (1, 0)$ and $\boldsymbol{e}_y = (0, 1)$ being the unit vectors. Based on the point-group symmetry of the square lattice, we classify the η-pairing operators into those of the irreducible representations. Among them, the η-pairing operator with the $d_{x^2-y^2}$-wave (d-wave) pairing symmetry corresponds to

$$\eta_d^+ = \eta_{+e_x}^+ - \eta_{+e_y}^+ - \eta_{-e_x}^+ + \eta_{-e_y}^+. \tag{10}$$

The minus sign in the second term relative to the first term in Eq. (10) indicates the d-wave symmetry, while the minus sign in the third term relative to the first term reflects the spin-singlet pairing [69]. For other pairing states (such as those having s-, p_x-, and p_y-wave symmetries) which can also be created by the off-site η-pairing operators, we refer to Sec. V A. Using the η-pairing operator η_d^+, we can define the d-wave η-pairing state as

$$|\Psi_d^N\rangle = \frac{1}{\mathcal{N}_d^N}(\eta_d^+)^{N/2}|0\rangle, \tag{11}$$

where N is the number of fermions (which is even), and $\mathcal{N}_d^N$ is the normalization constant (such that $\langle\Psi_d^N|\Psi_d^N\rangle = 1$).

C. Hubbard model with the two-body interaction

To seek for a lattice model in which the d-wave η-pairing state becomes an eigenstate, let us first consider the ordinary two-dimensional spinful Hubbard model with the two-body interaction. The Hamiltonian is written as

$$\mathcal{H}_{\mathrm{H}} = \mathcal{H}_{\mathrm{kin}} + \mathcal{H}_U, \tag{12}$$

$$\mathcal{H}_{\mathrm{kin}} = -t\sum_{\langle i,j\rangle\sigma} c_{i\sigma}^\dagger c_{j\sigma}, \tag{13}$$

$$\mathcal{H}_U = U\sum_i n_{i\uparrow}n_{i\downarrow}. \tag{14}$$

Here, $\langle i,j\rangle$ represents the sum over a pair of nearest-neighbor sites, $c_{i\sigma}$ is a short-hand notation of $c_{\bm{r}_i,\sigma}$, and $n_{i\sigma} = c_{i\sigma}^\dagger c_{i\sigma}$ is the number operator. The term $\mathcal{H}_{\mathrm{kin}}$ (Eq. (13)) describes the nearest-neighbor hopping with t being the transfer integral, and the term $\mathcal{H}_U$ (Eq. (14)) represents the on-site two-body interaction with the strength U.

One can quickly see that η-pairing states created by the off-site η-pair operators $\eta_{\bm{\alpha}}^+$ in Eq. (9) are zero-energy eigenstates of $\mathcal{H}_{\mathrm{kin}}$ in Eq. (13) under the periodic boundary condition: we can rewrite the kinetic term and the η-pairing operator in the momentum basis as $\mathcal{H}_{\mathrm{kin}} = \sum_{\bm{k}\sigma} \varepsilon(\bm{k})c_{\bm{k}\sigma}^\dagger c_{\bm{k}\sigma}$ and $\eta_{\bm{\alpha}}^+ = \sum_{\bm{k}} \exp(-i\bm{k}\cdot\bm{\alpha})c_{\bm{\pi}-\bm{k},\uparrow}^\dagger c_{\bm{k},\downarrow}^\dagger$, where $\varepsilon(\bm{k}) = -2t(\cos k_x + \cos k_y)$ is the dispersion relation for the square lattice, $c_{\bm{k}\sigma} = (L_x L_y)^{-1/2}\sum_i c_{\bm{r}_i\sigma}\exp(-i\bm{k}\cdot\bm{r}_i)$ is the Fourier transformed form of the annihilation operator with crystal momentum $\bm{k}$, and L_x (L_y) is the system length in the x (y) direction. One can immediately see that $[\mathcal{H}_{\mathrm{kin}}, \eta_{\bm{\alpha}}^+] = \sum_{\bm{k}} \exp(-i\bm{k}\cdot\bm{\alpha})\,(\varepsilon(\bm{k}) + \varepsilon(\bm{\pi}-\bm{k}))c_{\bm{\pi}-\bm{k},\uparrow}^\dagger c_{\bm{k},\downarrow}^\dagger = 0$, since the dispersion relation satisfies $\varepsilon(\bm{k}) + \varepsilon(\bm{\pi} - \bm{k}) = 0$. Hence, the d-wave η-pairing state $|\Psi_d^N\rangle$ in Eq. (11) is a zero-energy eigenstate for the kinetic term,

$$\mathcal{H}_{\mathrm{kin}}|\Psi_d^N\rangle = 0, \tag{15}$$

on the square lattice with the periodic boundary condition. We note that any pairing states created by $\eta_{\bm{\alpha}}^+$ (including s-, p_x-, and p_y-wave pairing symmetries) are also eigenstates of $\mathcal{H}_{\mathrm{kin}}$.

Next, we look at the interaction term $\mathcal{H}_U$ in Eq. (14), for which we take the coordinate-space representation in the Fock
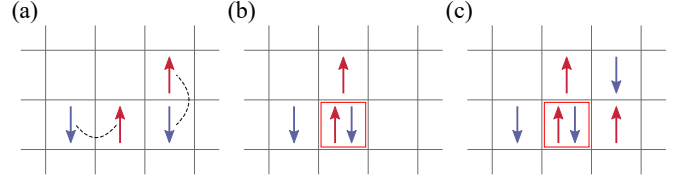

FIG. 2. Examples of Fock states included in the d-wave η-pairing state (Eq. (11)) on the square lattice: The case of (a) two pairs (connected by dashed curves) separated to each other, (b) two pairs overlapped to each other to form a doublon (enclosed by a red square), and (c) three pairs having a doublon surrounded by more than two particles. Red (blue) arrows represent particles with spin up (down).

basis. Given a set of occupation numbers $\{\nu_{i\sigma}\}$, where $\nu_{i\sigma}$ (= 0, 1) denotes the number of spin-σ particles at site i, a Fock state is represented by

$$|\{\nu_{i\sigma}\}\rangle = \prod_i \left(c_{i\sigma}^\dagger\right)^{\nu_{i\sigma}}|0\rangle. \tag{16}$$

The d-wave η-pairing state is expanded as a linear combination of Fock states in which various oriented pairs are distributed on the square lattice. Examples of those Fock states are shown in Fig. 2. When two off-site pairs are present, they are either un-overlapped or overlapped, as shown in Fig. 2(a) and (b), respectively. In the latter case, a doublon is formed, generating an energy cost due to the on-site two-body interaction. This means that the latter Fock basis (Fig. 2(b)) has higher interaction energy (with the difference U) than the former basis (Fig. 2(a)). Therefore, the d-wave η-pairing state $|\Psi_d^N\rangle$ in Eq. (11) is not an energy eigenstate of $\mathcal{H}_U$ (Eq. (14)). When three (or more) pairs exist, more than two particles can occupy nearest-neighbor sites of a doublon, as shown in Fig. 2(c). This example indicates that a naive application of the three-body interaction introduced in Sec. II A is not sufficient to cancel the energy increment of the d-wave pairs due to the formation of doublons. The question is how such an energy change can be cancelled for all possible configurations of off-site pairs.

D. Hubbard model with multi-body interactions

Here we show that the unconventional η-pairing states can become exact energy eigenstates by introducing generalized multi-body interactions to the Hubbard model. As mentioned before, our motivation is to cancel the energy increment due to the formation of doublons by the multi-body interactions. Since the number of particles that surround a doublon may vary depending on the configurations of pairs (see Fig. 2), it will be convenient to introduce an operator that judges whether neighboring sites (next to a doublon) are occupied by particles or not. This allows us to efficiently measure how much energy should be subtracted for each pair configuration to make the unconventional η-pairing states exact eigenstates.

Such an operator, denoted by $\mathbb{n}_{i\sigma}$, is defined as follows. In the coordinate basis spanned by Fock states in Eq. (16), the
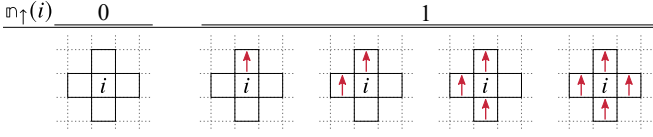
FIG. 3. Values of the neighboring particle existence operator $\mathbb{n}_{i\sigma}$ in Eq. (17) with $\sigma =\uparrow$ for each configuration of spin-up particles (red arrows) at the nearest-neighbors sites of site i. When there are no particles around site i, the operator takes a value of 0. Otherwise, if particles exist around site i, the operator takes a value of 1.

operator $\mathbb{n}_{i\sigma}$ takes a value of 0 or 1 in such a way as

$$
\mathbb{n}_{i\sigma} = \begin{cases} 1 & (n_{\mathrm{nn}(i)\sigma} \neq 0) \\ 0 & (n_{\mathrm{nn}(i)\sigma} = 0) \end{cases}, \tag{17}
$$

where $n_{\mathrm{nn}(i)\sigma}$ is the total number of spin-σ particles occupying the nearest-neighbor sites of site i (denoted by nn(i)). We call the operator $\mathbb{n}_{i\sigma}$ the neighboring particle existence operator. In the case of the square lattice, we show the values of $\mathbb{n}_{i\sigma}$ (with $\sigma =\uparrow$) for each configuration of spin-up particles around site i in Fig. 3. Note that the values of $\mathbb{n}_{i\sigma}$ do not depend on the configuration of particles with the opposite spin $\bar{\sigma}$. The operator in Eq. (17) tells us the presence (or absence) of a particle in the vicinity of a target site i, which can be used to avoid overcounting the number of neighboring particles, as described below.

The operator $\mathbb{n}_{i\sigma}$ in Eq. (17) is explicitly represented as a combination of multiples of the ordinary number operator $n_{i\sigma}$. Let us label the nearest-neighbor sites of site i by $i_1, i_2, \ldots, i_z$, where z is the coordination number of the lattice. Then $\mathbb{n}_{i\sigma}$ can be written as

$$
\begin{aligned}
\mathbb{n}_{i\sigma} &= 1 - \prod_{m=1}^{z}(1 - \hat{n}_{i_m\sigma}) \\
&= -\sum_{m=1}^{z}(-1)^m \sideset{}{'}\sum_{j_1,\cdots,j_m \in \mathrm{nn}(i)} \hat{n}_{j_1\sigma} \cdots \hat{n}_{j_m\sigma},
\end{aligned} \tag{18}
$$

where the prime summation means that j_l ($l = 1, \cdots, m$) runs over the nearest-neighbor sites of site i with $j_l \neq j_{l'}$ ($l < l'$), and different orders of $(j_1, j_2, \cdots, j_m)$ are not double-counted. In general, $\mathbb{n}_{i\sigma}$ contains m-body operators with $1 \leq m \leq z$. The representation (Eq. (18)) is applicable to arbitrary lattice structures.

In order to get an insight of how to cancel the energy increment of doublons with multi-body interations, we take two examples of Fock states relevant to the unconventional η-pairing states: One is the case where two pairs are overlapped to each other to form a doublon, as shown in Fig. 4(a). The other is the case where there is another pair in the vicinity of the two pairs, as shown in Fig. 4(b). We label the site occupied by the doublon by i. As shown in Fig. 4(a), there are always two residual particles from the pairs that form the doublon, so that we can cancel the on-site two-body interaction $Un_{i\uparrow}n_{i\downarrow}$ by adding the following three-body interaction between the doublon and a
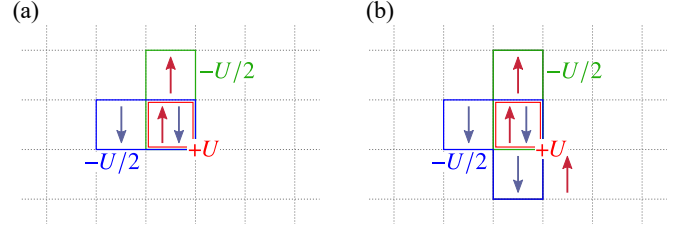

FIG. 4. Interactions between off-site pairs in the d-wave η-pairing state in a spinful model with spin-$\uparrow$ (spin-$\downarrow$) particles indicated by the red (blue) arrows. (a) When two pairs are overlapped with each other to form a doublon, the on-site two-body interaction is cancelled by the three-body interaction (Eq. (19)) acting between the doublon and a single particle. (b) When another pair comes next to the doublon, the on-site two-body interaction is not cancelled by the three-body interaction (Eq. (19)), but is cancelled by the multi-body interaction in the form of Eq. (20). Two particles forming a doublon are indicated by the red squares, while the multi-body interacting doublon and spin-$\uparrow$ (spin-$\downarrow$) particles are enclosed by the blue (green) boxes.

particle,

$$
-\frac{U}{2} \sum_{j \in \mathrm{nn}(i), \sigma} n_{i\uparrow}n_{i\downarrow}n_{j\sigma}, \tag{19}
$$

where j runs over the nearest-neighbor sites of site i. In Fig. 4(b), however, the three-body interaction given by Eq. (19) amounts to $-3U/2$, which does not perfectly cancel the on-site two-body interaction U. This is due to the overcounting of the three-body interaction energy from the neighboring pairs. To avoid this overcounting, we replace $\sum_{j \in \mathrm{nn}(i)} n_{j\sigma}$ by $\mathbb{n}_{i\sigma}$ in Eq. (17) as follows:

$$
-\frac{U}{2} \sum_{\sigma} n_{i\uparrow}n_{i\downarrow}\mathbb{n}_{i\sigma}. \tag{20}
$$

The multi-body interaction (Eq. (20)) contains M-body interactions with $3 \leq M \leq z+2$. With this form of the multi-body interaction, it is possible to incorporate only the interaction between the doublon and a single spin-$\uparrow$ particle, and the interaction between the doublon and a single spin-$\downarrow$ particle. One can see that the cancellation between the on-site two-body interaction $\mathcal{H}_U$ (Eq. (14)) and the multi-body interaction (Eq. (20)) works not only for the cases of Fig. 4(a) and (b) but also for *all the possible configurations of pairs* in the unconventional η-pairing states, which can be easily checked since the cancellation occurs for each doublon one by one.

Based on the multi-body interaction in Eq. (20) introduced above, we define an extended Hubbard model having the unconventional η-pairing states as energy eigenstates. The Hamiltonian of the extended Hubbard model, denoted by $\mathcal{H}_{\mathrm{extH}}$, is given as follows:

$$
\mathcal{H}_{\mathrm{extH}} = \mathcal{H}_{\mathrm{kin}} + \mathcal{H}_{\mathrm{int}}, \tag{21}
$$

$$
\mathcal{H}_{\mathrm{int}} = U \sum_{i} n_{i\uparrow}n_{i\downarrow}\left(1 - \frac{1}{2}\sum_{\sigma} \mathbb{n}_{i\sigma}\right). \tag{22}
$$

As discussed in the previous paragraph, the interaction energy is always zero for the unconventional η-pairing states, due

to the cancellation between the two-body interaction and the multi-body interaction (Eq. (20)). In particular, the d-wave η-pairing state $|\Psi_d^N\rangle$ in Eq. (11) is an exact eigenstate of $\mathcal{H}_{\text{extH}}$ with a zero eigenenergy,

$$\mathcal{H}_{\text{extH}}|\Psi_d^N\rangle = 0. \qquad (23)$$

We remark that arbitrary η-pairing states created by η_α^+ are also eigenstates of $\mathcal{H}_{\text{extH}}$ (see Sec. V A). The same form of the Hamiltonian can be used for other bipartite lattices in arbitrary dimensions (e.g., the honeycomb lattice, the diamond lattice, etc.) to include unconventional η-pairing states as eigenstates. The lattice structure must be bipartite, since the η-pairing states have staggered phases in real space in order to be eigenstates of the kinetic term $\mathcal{H}_{\text{kin}}$. Some of the examples are shown in Sec. V.

Let us mention the relationship between our construction and previously proposed frameworks of QMBS states. The obtained Hamiltonian $\mathcal{H}_{\text{extH}}$ in Eq. (21) satisfies the restricted spectrum-generating algebra [30] in the Hilbert space spanned by a series of the d-wave η-pairing states $\{|\Psi_d^N\rangle \mid N = 2, 4, \cdots\}$. However, as shown in Eq. (18), the Hamiltonian $\mathcal{H}_{\text{extH}}$ contains terms up to six-body density-density interactions in the case of the square lattice. The conventional approach of assuming interaction forms and adjusting interaction coefficients to satisfy the restricted spectrum-generating algebra would be impractical due to the complexity of the commutation relations with the d-wave η-pairing operator in Eq. (10). The advantage of our approach is that we can systematically and directly construct model Hamiltonians that have off-site pair condensed states with unconventional pairing symmetry as their eigenstates in systems of higher dimensions and including spin degrees of freedom.

III. PHYSICAL PROPERTIES OF THE UNCONVENTIONAL η-PAIRING STATES

In this section, we numerically confirm the nonthermal nature of the unconventional η-pairing states by computing two physical quantities: the superconducting correlation function and the entanglement entropy. To obtain these quantities, we numerically calculated the entire exact wavefunction of the d-wave η-pairing state (Eq. (11)) on a $L_x \times L_y$ square lattice with the periodic boundary condition.

A. Off-diagonal long-range order

We examine the nearest-neighbor pair correlation functions for the d-wave η-pairing state defined by

$$C_{\alpha\beta}(\boldsymbol{r}) = \langle \Psi_d^N | c_{\boldsymbol{r}+\boldsymbol{e}_\alpha\downarrow}^\dagger c_{\boldsymbol{r}\uparrow}^\dagger c_{\boldsymbol{0}\uparrow} c_{\boldsymbol{e}_\beta\downarrow} | \Psi_d^N \rangle, \qquad (24)$$

where the subscripts α and β $(= x, y)$ denote the orientation direction of the pairs, and $\boldsymbol{r}$ corresponds to the relative displacement between up-spin particles. We consider a quarter-filled system with the lattice length $L_y = 4$ and $L_x = 4, 6, 8$
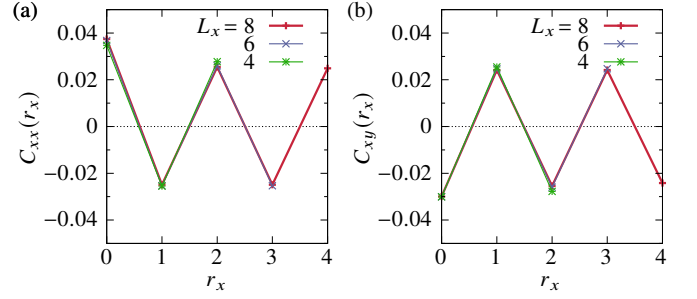

FIG. 5. Pair correlation functions in Eq. (24) of the d-wave η-pairing state on the $L_x \times L_y$ lattice with $L_x = 4, 6, 8$ and $L_y = 4$. (a) The correlation between x-oriented pairs and (b) the correlation between x-oriented and y-oriented pairs as a function of a distance r_x between pairs along the x axis.

($N = 4, 6, 8$). From the orientation dependence of the long-range pair correlations, one can discriminate different pairing symmetries.

Figure 5 shows the calculated pair correlation functions as a function of the distance along the x axis (i.e., we set $\boldsymbol{r} = r_x \boldsymbol{e}_x$), where Figs. 5(a) and (b) correspond to the parallel and orthogonal pair orientations, respectively. We observe the staggered oscillations for both of the orientations, which do not quickly decay in a long distance (within the system size). This is a direct consequence of the fact that the pairs carry a momentum $\boldsymbol{\pi}$ (and hence the staggered phase) in the η-pairing states in Eq. (9). We also see that the results of the pair correlations are well converged with respect to the system size with the particle density being fixed, implying that the off-diagonal long-range order is present for the d-wave η-pairing state. If one compares Fig. 5(a) with Fig. 5(b), one finds that the sign is reversed with respect to the pair orientation. This reflects the d-wave pairing symmetry.

B. Entanglement entropy

Next, we verify a nonthermal behavior of the d-wave η-pairing state through the entanglement entropy. We consider the same $L_x \times L_y$ lattice as in the previous subsection with the periodic boundary condition. The entire system (a torus) is divided into subsystems A and B (two tubes), where A has the size of $r_x \times L_y$. The entanglement entropy for the d-wave η-pairing state in Eq. (11) is defined by $S_A(|\Psi_d^N\rangle) = -\text{Tr}_A[\rho_A \ln \rho_A]$, where ρ_A is the reduced density matrix for the subsystem A, i.e., $\rho_A = \text{Tr}_B[|\Psi_d^N\rangle\langle\Psi_d^N|]$. We compute $S_A(|\Psi_{N,d}\rangle)$ as a function of the volume fraction $f = V_A/V$, where $V = 2L_x L_y$ ($V_A = 2r_x L_y$) is the product of the system (subsystem) volume and the spin degrees of freedom.

The entanglement entropy of typical eigenstates of nonintegrable (chaotic) systems is expected to behave as the average entanglement entropy of a quantum pure-state ensemble, while that of integrable systems is to behave as that of a pure Gaussian state ensemble [70]. In nonintegrable systems, the average entanglement entropy of a uniformly distributed pure state in a particle number conserving
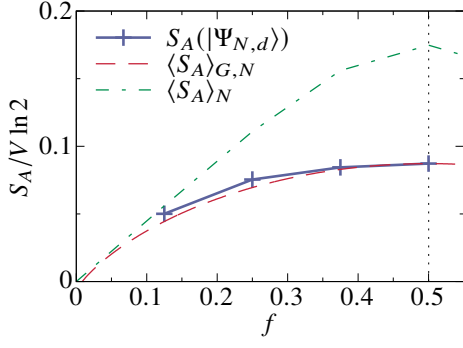
FIG. 6. Entanglement entropy for fermionic systems on the $L_x \times L_y$ lattice as a function of the volume fraction $f = V_A/V$ with $L_x = 8$, $L_y = 4$, and the particle number $N = 6$. The blue cross points show the entanglement entropy of the d-wave η-pairing state. The red dashed (green chained) curve represents the average entanglement entropy $\langle S_A \rangle_{G,N}$ ($\langle S_A \rangle_N$) typically obtained for a energy eigenstate in integrable (nonintegrable) systems.
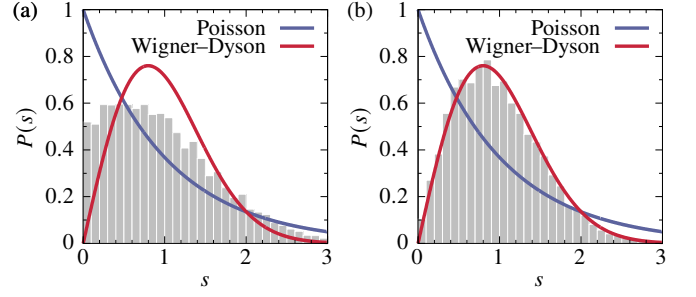

FIG. 7. Nearest-neighbor level-spacing distribution $P(s)$ (shown by the histograms) for the extended Hubbard model with the multi-body interactions (Eq. (21)) on the square lattice with the quantum numbers (a) $(\mathcal{P}_x, \mathcal{P}_y, \mathcal{P}_d) = (+1, +1, +1)$ and (b) $(+1, +1, -1)$. The parameters are set to be $L_x = L_y = 4$, $N = 8$, and $U/t = 2$. The blue and red curves correspond to the Poisson and Wigner-Dyson distributions, respectively.

Hilbert space for a fermionic system is given by $\langle S_A \rangle_N = \sum_{N_A=0}^{\min(N, V_A)} [\langle S_A \rangle + \psi(d_N + 1) - \psi(d_A d_B + 1)] d_A d_B/d_N$, where N_A is the particle number in the subspace A, $\langle S_A \rangle = \psi(d_A d_B + 1) - \psi(d_A + 1) - (d_B - 1)/2 d_A$ is the Page formula in $d_A > d_B$ [71], $\psi(x)$ is the digamma function, and $d_N = \binom{V}{N}$, $d_A = \binom{V_A}{N_A}$, and $d_B = \binom{V - V_A}{N - N_A}$ are the Hilbert-space dimensions of the entire system, subspace A, and complementary subspace B, respectively. Similarly, in integrable systems, the average entanglement entropy over all pure fermionic Gaussian states in the thermodynamic limit is given by $\langle S_A \rangle_{G,N} = V \{(n - 1) \ln(1 - n) + n[(f - 1) \ln(1 - f) - f \ln f - 1]\}$ [70], where $n = N/V$ is the up-spin (or down-spin) particle density.

Figure 6 shows the calculated entanglement entropy for the d-wave η-pairing state indicated by the blue cross points. We also show the average entanglement entropy $\langle S_A \rangle_N$ and $\langle S_A \rangle_{G,N}$ with red dashed and green chained curves, respectively. We observe that the entanglement entropy of the d-wave η-pairing state increases as the subsystem volume increases. Particularly, we found that the subsystem size dependence of the entanglement entropy is in quantitative agreement with that typically observed in integrable systems, which is substantially smaller than the typical entanglement entropy in nonintegrable systems. These numerical results support the nonthermal property of the d-wave η-pairing state.

IV. NONINTEGRABILITY OF THE MULTI-BODY INTERACTING MODEL

In this section, we numerically confirm the nonintegrability of the extended Hubbard model $\mathcal{H}_{\mathrm{extH}}$ in Eq. (21) from the energy level statistics. Combining the results with those of Sec. III, we can judge whether the d-wave η-pairing state in the model is identified to be a QMBS state or not. If the distribution of the difference between the nearest-neighbor eigenenergies follows the Wigner-Dyson distribution $P_{\mathrm{WD}}(s) = (\pi/2)s \exp(-\pi s^2/4)$ with s being the level spacing,

then the model is suggested to be nonintegrable and all the other energy eigenstates are thermal as expected from the argument of the ETH.

We consider the extended Hubbard model in Eq. (21) on the square lattice under the periodic boundary condition with $L_x = L_y = 4$, $N = 8$, and the total magnetization $S^z = 0$. We utilize the Lanczos method to numerically diagonalize the Hamiltonian. Since the Hamiltonian has several global symmetries, we select a target subspace using symmetry projection operators. As internal symmetries, we consider the time-reversal ($\mathcal{T}$) and spin-rotation symmetries. It should be noted that our multi-body interacting system does not have the particle-hole symmetry, unlike the two-body interacting Hubbard model in Eq. (12). Among the elements of the point group C_{4v} (which is the symmetry of the square lattice), we take the reflections $\mathcal{P}_x$, $\mathcal{P}_y$, and $\mathcal{P}_d$ with respect to the x-, y-, and diagonal axes, respectively. Additionally, the system has the translation symmetries $\mathcal{X}$ and $\mathcal{Y}$ along the x and y directions, respectively. We focus on the subspaces in which the d-wave η-pairing state exists, namely with $\mathcal{T} = +1$, the total spin $S = 0$, $(\mathcal{P}_x, \mathcal{P}_y, \mathcal{P}_d) = (+1, +1, +1)$ and $(-1, -1, +1)$, and the total momentum $(0, 0)$ [72]. Note that in a 4×4 periodic lattice system, there is an accidental hidden symmetry, i.e., the four-dimensional hypercubic symmetry [73]. If this higher symmetry is not taken into account to define the target space, the level-spacing distributions may behave differently from the Wigner-Dyson distribution (even though the system might be nonintegrable), which will be discussed later.

Figure 7(a) shows the nearest-neighbor level-spacing distribution $P(s)$ in the subspace with the quantum numbers $(\mathcal{P}_x, \mathcal{P}_y, \mathcal{P}_d) = (+1, +1, +1)$, where we adopt the unfolding method with the Gaussian kernel density estimation [74] with the smoothing parameter $\sigma_{\mathrm{Gauss}} = 0.1$. We find that the obtained level-spacing distribution has a shape in between the Poisson distribution $P_{\mathrm{P}}(s) = \exp(-s)$ and the Wigner-Dyson distribution $P_{\mathrm{WD}}(s)$. A similar behavior is often observed when an extra discrete symmetry remains to be considered in a nonintegrable model. For example, in the two-body interacting Hubbard model (Eq. (12)) on the same 4×4 periodic

lattice, the level-spacing distribution has been found to be neither the Poisson nor Wigner-Dyson distribution [73]. As we remarked before, this is due to the presence of the accidental hypercubic symmetry for the 4×4 lattice geometry, which has not been taken into account in the level-spacing analysis. Such an intermediate distribution between the Poisson and Wigner-Dyson ones has been reproduced by a spectrum of two independent GOE samples in the random matrix theory mixed with appropriate weights [73]. We also examine the subspace with another set of the quantum numbers $(\mathcal{P}_x, \mathcal{P}_y, \mathcal{P}_d) = (+1, +1, -1)$, and obtain the level-spacing distribution as shown in Fig. 7(b). We observe that the spectrum is in good agreement with the Wigner-Dyson distribution. Based on these results, we conclude that the multi-body interacting model (Eq. (21)) is nonintegrable.

Given the above results with the nonthermal properties of the eigenstate seen in Sec. III, the d-wave η-pairing state (Eq. (11)) can be regarded as a QMBS state in the nonintegrable system (Eq. (21)). The basic principle that makes the unconventional η-pairing states QMBSs is to use multi-body interactions to protect the pairs from having the energy increase due to the two-body interaction.

V. GENERALIZATIONS

In this section, we present several generalizations of our approach to construct superconducting scar states with the multi-body interactions: generalized off-site η-pairing states (Sec. V A), f-wave η-pairing states on the honeycomb lattice (Sec. V B), s-wave η-pairing states in a nearest-neighbor interacting system (Sec. V C), and p-wave η-pairing states in the one-dimensional spinless fermion system (Sec. V D).

A. General pairing symmetry and long-range pairing

The extended Hubbard model with the multi-body interactions in Eq. (21) has not only the d-wave η-pairing state but also several other η-pairing states with different pairing symmetries as energy eigenstates, since the energy cancellation holds for each Fock basis. Let us consider s-, p_x-, and p_y-wave pairing symmetries, for which η-pairing operators are defined by

$$\eta_s^+ = \eta_{+e_x}^+ + \eta_{+e_y}^+ - \eta_{-e_x}^+ - \eta_{-e_y}^+, \quad (25)$$

$$\eta_{p_x}^+ = \eta_{+e_x}^+ + \eta_{-e_x}^+, \quad (26)$$

$$\eta_{p_y}^+ = \eta_{+e_y}^+ + \eta_{-e_y}^+, \quad (27)$$

respectively. Acting each operator multiple times to the vacuum state $|0\rangle$ yields the s-, p_x-, and p_y-wave η-pairing states, as in the case of the d-wave symmetry. Since these η-pairing states are represented by the same set of Fock bases in which the nearest-neighbor pairs are distributed, they are also energy eigenstates of $\mathcal{H}_{\text{extH}}$ with zero eigenenergies, and hence are QMBS states.

Moreover, one can also combine these η-pairing operators with different pairing symmetries to define general η-pairing

states,

$$|\nu_s \nu_{p_x} \nu_{p_y} \nu_d\rangle \propto \left(\eta_s^+\right)^{\nu_s} \left(\eta_{p_x}^+\right)^{\nu_{p_x}} \left(\eta_{p_y}^+\right)^{\nu_{p_y}} \left(\eta_d^+\right)^{\nu_d} |0\rangle, \quad (28)$$

where ν_γ ($\gamma = s, p_x, p_y, d$) denotes the number of pairs with the γ-wave pairing symmetry. These η-pairing states are eigenstates of $\mathcal{H}_{\text{extH}}$ in Eq. (21), and are degenerate at zero energy. Note that an arbitrary linear combination of the general η-pairing states (Eq. (28)) is also an eigenstate of $\mathcal{H}_{\text{extH}}$ in Eq. (21), since they are all degenerate at zero energy. In order to induce the d-wave η-pairing state by a certain excitation protocol, it will be better if the d-wave pairing state is energetically separated from the other degenerate states. In this paper, we leave how to break the degeneracy an open issue.

While we have focused on the two-dimensional square lattice so far, most of the results can be straightforwardly extended to other dimensions and other bipartite lattice systems. The bipartite lattice condition is necessary for the η-pairing states to be eigenstates of the kinetic term $\mathcal{H}_{\text{kin}}$ (Eq. (13)). We can define the interaction term $\mathcal{H}_{\text{int}}$ (Eq. (22)) and the neighboring particle existence operator $\mathbb{n}_{i\sigma}$ in Eqs. (17) and (18) irrespective of dimensions and lattice structures. Therefore, one can use the Hamiltonian (Eq. (21)), for example, on the honeycomb, body-centered-cubic, and diamond lattices. The case of the honeycomb lattice is described in Sec. V B.

We can also generalize our construction to cases of long-range pairs. Let α refer to the n-th nearest-neighbor sites around site i, which is denoted by $\alpha \in \text{nn}(n, i)$. The long-range η-pairing states are defined by $(\eta_\alpha^+)^{N/2}|0\rangle$ with $\alpha \in \text{nn}(n, i)$. The case of $n = 1$ corresponds to the previous results. In the square lattice, $\alpha = \pm e_x \pm e_y$ when $n = 2$, and $\alpha = \pm 2e_x, \pm 2e_y$ when $n = 3$. The multi-body interaction takes the same form of $n_{i\uparrow} n_{i\downarrow} \mathbb{n}_{i\sigma}$ but with

$$\mathbb{n}_{i\sigma} = \begin{cases} 1 & (n_{\text{nn}(n,i)\sigma} \neq 0) \\ 0 & (n_{\text{nn}(n,i)\sigma} = 0) \end{cases}, \quad (29)$$

where $n_{\text{nn}(n,i)\sigma}$ is the number of spin-σ particles on $\text{nn}(n, i)$. In this way, the η-pairing states with the long-range pairs also become energy eigenstates due to the longer-range multi-body interaction. It should be noted that our method of realizing superconducting scar states using multi-body interactions is only applicable to pairs of particles separated by a fixed distance.

B. f-wave η-pairing state on the honeycomb lattice

Let us consider the multi-body interacting model defined by Eq. (21) on the honeycomb lattice, where an η-pairing state with the f-wave pairing symmetry becomes an eigenstate (see Fig. 1(c)). The lattice structure is defined as follows. We label sublattices by A and B, as shown in Fig. 8(a). Let τ_γ ($\gamma = 1, 2, 3$) be the bond vectors and R_γ the lattice vectors, which are explicitly given by

$$\tau_1 = \begin{pmatrix} 0 \\ 1/\sqrt{3} \end{pmatrix}, \tau_2 = \begin{pmatrix} -1/2 \\ -1/2\sqrt{3} \end{pmatrix}, \tau_3 = \begin{pmatrix} 1/2 \\ -1/2\sqrt{3} \end{pmatrix}, \quad (30)$$

$$R_1 = \tau_3 - \tau_2, \quad R_2 = \tau_1 - \tau_3, \quad R_3 = \tau_2 - \tau_1. \quad (31)$$
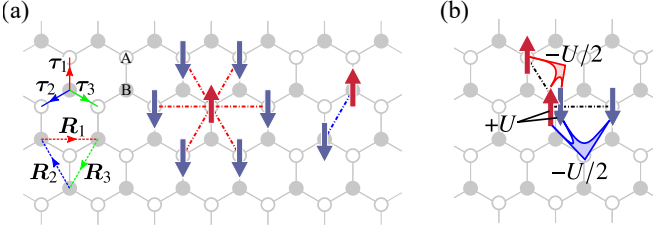
FIG. 8. Generalized η-pairing states on the honeycomb lattice. (a) Six kinds of next-nearest-neighbor pairs (connected by the dash-dotted lines) in the η-pairing states. The white (grey) circles represent A (B) sublattice sites. $\boldsymbol{\tau}_\gamma$ and $\boldsymbol{R}_\gamma$ ($\gamma = 1, 2, 3$) denote the bond and lattice vectors, respectively. A pair on the B sublattice (connected by the blue dash-dotted line) has the opposite sign of the wavefunction with respect to those on the A sublattice. (b) Energy cancellation between the two-body (black lines) and multi-body (filled areas) interactions acting on overlapped pairs.

The Fourier transform of the annihilation operator $c_{i\sigma}^l$ of fermions for each sublattice l (= A, B) is given by $c_{i\sigma}^l = N_s^{-1/2} \sum_{\boldsymbol{k}} \exp(\mathrm{i}\boldsymbol{k} \cdot \boldsymbol{r}_i) c_{\boldsymbol{k}\sigma}^l$ with N_s being the total number of unit cells. After the Fourier transformation, the kinetic Hamiltonian in Eq. (13) is diagonalized as

$$\mathcal{H}_{\mathrm{kin}} = \sum_{\boldsymbol{k}\sigma} \left(c_{\boldsymbol{k}\sigma}^{A\ \dagger}, \ c_{\boldsymbol{k}\sigma}^{B\ \dagger} \right) \begin{pmatrix} 0 & g(\boldsymbol{k}) \\ g^*(\boldsymbol{k}) & 0 \end{pmatrix} \begin{pmatrix} c_{\boldsymbol{k}\sigma}^{A} \\ c_{\boldsymbol{k}\sigma}^{B} \end{pmatrix}, \quad (32)$$

$$= \sum_{\boldsymbol{k}\sigma} |g(\boldsymbol{k})| \left[c_{\boldsymbol{k}\sigma}^{(+)\ \dagger} c_{\boldsymbol{k}\sigma}^{(+)} - c_{\boldsymbol{k}\sigma}^{(-)\ \dagger} c_{\boldsymbol{k}\sigma}^{(-)} \right], \quad (33)$$

where the hopping amplitude $g(\boldsymbol{k})$ and the creation operators of the energy eigenstates labeled by $(+)$ and $(-)$ are given by

$$g(\boldsymbol{k}) = \sum_{\gamma=1,2,3} e^{\mathrm{i}\boldsymbol{k}\cdot\boldsymbol{\tau}_\gamma}, \quad (34)$$

$$\left(c_{\boldsymbol{k}\sigma}^{(+)\ \dagger}, \ c_{\boldsymbol{k}\sigma}^{(-)\ \dagger} \right) = \left(c_{\boldsymbol{k}\sigma}^{A\ \dagger}, \ c_{\boldsymbol{k}\sigma}^{B\ \dagger} \right) \frac{1}{\sqrt{2}|g(\boldsymbol{k})|} \begin{pmatrix} g(\boldsymbol{k}) & g(\boldsymbol{k}) \\ |g(\boldsymbol{k})| & -|g(\boldsymbol{k})| \end{pmatrix}, \quad (35)$$

respectively.

The off-site η-pairing operators on the honeycomb lattice are defined in the same way as in Eq. (9):

$$\eta_{\boldsymbol{\alpha}}^+ = \sum_i f(\boldsymbol{r}_i) c_{\boldsymbol{r}_i,\uparrow}^\dagger c_{\boldsymbol{r}_i+\boldsymbol{\alpha},\downarrow}^\dagger, \quad (36)$$

$$f(\boldsymbol{r}_i) = \begin{cases} 1 & (\boldsymbol{r}_i \in A), \\ -1 & (\boldsymbol{r}_i \in B), \end{cases} \quad (37)$$

where $f(\boldsymbol{r}_i)$ is the counterpart of the phase factor $\exp(\mathrm{i}\boldsymbol{\pi} \cdot \boldsymbol{r}_i)$ in the case of the square lattice in Eq. (9), and $\boldsymbol{r}_i \in A$ (B) indicates that the site i belongs to the sublattice A (B). The direction vector of the pairs is given by $\boldsymbol{\alpha} = \pm\boldsymbol{R}_\gamma$, where $\boldsymbol{\alpha}$ is at the second nearest-neighbor sites, namely $\boldsymbol{\alpha} \in \mathrm{nn}(2, i)$. These six η-pairing operators create the next-nearest neighbor pairing states with the staggered phase factors, as shown in Fig. 8(a).

The unconventional η-pairing states on the honeycomb lattice are also defined by using the η-pairing operators in

Eq. (36). As an example, we introduce an η-pairing state with the f-wave pairing symmetry as follows:

$$\eta_f^+ = \eta_{+\boldsymbol{R}_1}^+ - \eta_{-\boldsymbol{R}_3}^+ + \eta_{+\boldsymbol{R}_2}^+ + \eta_{-\boldsymbol{R}_1}^+ - \eta_{+\boldsymbol{R}_3}^+ + \eta_{-\boldsymbol{R}_2}^+, \quad (38)$$

$$|\Psi_f^N\rangle \propto \left(\eta_f^+ \right)^{N/2} |0\rangle. \quad (39)$$

The following discussion also holds for other pairing symmetries as discussed in Sec. V A.

The η-pairing operators on the honeycomb lattice commute with the kinetic Hamiltonian $\mathcal{H}_{\mathrm{kin}}$ in Eqs. (32) and (33). In the momentum representation, the η-pairing operators in Eq. (36) are expressed as

$$\eta_{\boldsymbol{\alpha}}^+ = \sum_{\boldsymbol{k}} e^{\mathrm{i}\boldsymbol{k}\cdot\boldsymbol{\alpha}} \left(c_{\boldsymbol{k},\uparrow}^{A\ \dagger} c_{-\boldsymbol{k},\downarrow}^{A\ \dagger} - c_{\boldsymbol{k},\uparrow}^{B\ \dagger} c_{-\boldsymbol{k},\downarrow}^{B\ \dagger} \right), \quad (40)$$

$$= \sum_{\boldsymbol{k}} e^{\mathrm{i}\boldsymbol{k}\cdot\boldsymbol{\alpha}} \left(c_{\boldsymbol{k},\uparrow}^{(+)\ \dagger} c_{-\boldsymbol{k},\downarrow}^{(-)\ \dagger} + c_{\boldsymbol{k},\uparrow}^{(-)\ \dagger} c_{-\boldsymbol{k},\downarrow}^{(+)\ \dagger} \right). \quad (41)$$

The commutation relation between $\mathcal{H}_{\mathrm{kin}}$ (Eq. (32)) and $\eta_{\boldsymbol{\alpha}}^+$ (Eq. (40)) are evaluated as

$$\left[\mathcal{H}_{\mathrm{kin}}, \eta_{\boldsymbol{\alpha}}^+ \right] = \sum_{\boldsymbol{k}} e^{\mathrm{i}\boldsymbol{k}\cdot\boldsymbol{\alpha}} \Big(g^*(\boldsymbol{k}) c_{\boldsymbol{k}\uparrow}^{B\ \dagger} c_{-\boldsymbol{k}\downarrow}^{A\ \dagger} + g^*(-\boldsymbol{k}) c_{\boldsymbol{k}\uparrow}^{A\ \dagger} c_{-\boldsymbol{k}\downarrow}^{B\ \dagger}$$
$$- g(\boldsymbol{k}) c_{\boldsymbol{k}\uparrow}^{A\ \dagger} c_{-\boldsymbol{k}\downarrow}^{B\ \dagger} - g(-\boldsymbol{k}) c_{\boldsymbol{k}\uparrow}^{B\ \dagger} c_{-\boldsymbol{k}\downarrow}^{A\ \dagger} \Big). \quad (42)$$

Given $g(\boldsymbol{k}) = g^*(-\boldsymbol{k})$, the first and fourth terms and the second and third terms cancel each other, indicating that $[\mathcal{H}_{\mathrm{kin}}, \eta_{\boldsymbol{\alpha}}^+] = 0$. This is also confirmed from the commutation relation between Eqs. (33) and (41) as $\left[\mathcal{H}_{\mathrm{kint}}, \eta_{\boldsymbol{\alpha}}^+ \right] = \sum_{\boldsymbol{k}} \exp(\mathrm{i}\boldsymbol{k}\cdot\boldsymbol{\alpha}) \left(|g(\boldsymbol{k})| - |g(-\boldsymbol{k})| \right) (c_{\boldsymbol{k},\uparrow}^{(+)\ \dagger} c_{-\boldsymbol{k},\downarrow}^{(-)\ \dagger} + c_{\boldsymbol{k},\uparrow}^{(-)\ \dagger} c_{-\boldsymbol{k},\downarrow}^{(+)\ \dagger}) = 0$. Therefore, the f-wave η-pairing state is a zero-energy eigenstate of the kinetic term in Eq. (13).

By applying the neighboring particle existence operator $\mathbb{n}_{i\sigma}$ defined in Eq. (29) to the case of $\mathrm{nn}(2, i)$, the f-wave η-pairing state also becomes an energy eigenstate of the Hamiltonian in Eq. (21). The energy increase due to the two-body interaction U is canceled by the multi-body interactions between a doublon and a next-nearest neighboring particle, as shown in Fig. 8(b). Therefore, using the multi-body interactions, we can realize the η-pairing states with unconventional pairing symmetries in various lattice systems.

C. Yang's s-wave η-pairing state in a nearest-neighbor interacting system

It has been known that Yang's η-pairing state no longer becomes an energy eigenstate if one adds nearest-neighbor interactions to the Hubbard model in Eq. (12). However, one can make Yang's η-pairing state the energy eigenstate in nearest-neighbor interacting systems by utilizing appropriate multi-body interactions like those discussed above. The following discussions in this subsection are applicable to systems in arbitrary dimensions.
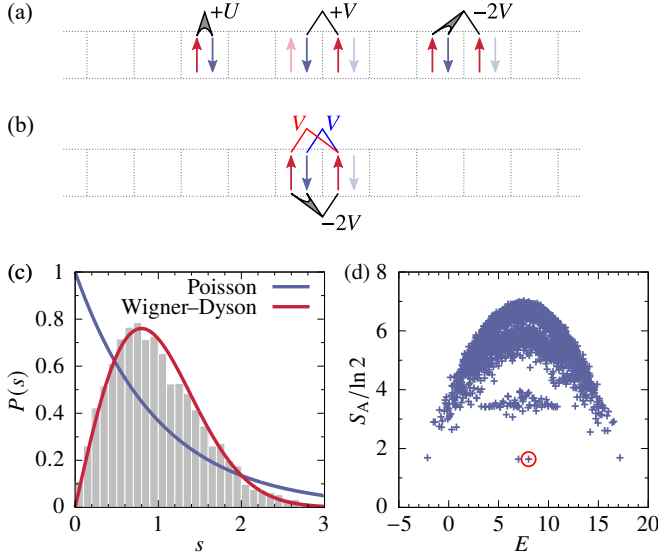
FIG. 9. (a) Interactions between doublons in Yang's s-wave η-pairing state in the model with the on-site interaction U and the nearest-neighbor two-body and three-body interactions in the form of Eq. (47). (b) Cancellation between the two-body and three-body interactions. (c) Nearset-neighbor level-spacing distribution $P(s)$ in the model $\mathcal{H}_\mathrm{H} + \mathcal{H}_{\mathrm{mod}V}$ with $L = 12$. (d) Entanglement entropy spectrum of the energy eigenstates in the corresponding model with $L = 8$. The red circle indicates Yang's η-pairing state. The parameters are set to be $t = 1$, $U = 2$, $V = 1$ and $N = L$.

Let us consider a d-dimensional periodic bipartite lattice, in which Yang's η-pairing state is defined as

$$\eta^+ = \sum_i e^{i\pi\cdot r_i} c_{i\uparrow}^\dagger c_{i\downarrow}^\dagger, \tag{43}$$

$$|\Psi^N\rangle = \frac{1}{\mathcal{N}^N}(\eta^+)^{N/2}|0\rangle, \tag{44}$$

with the normalization constant $\mathcal{N}^N$ (such that $\langle\Psi^N|\Psi^N\rangle = 1$). Yang's η-pairing state is a linear combination of Fock states with various configurations of doublons. It is known that this η-pairing state is the energy eigenstate of the Hubbard model (Eq. (12)), i.e., $\mathcal{H}_\mathrm{H}|\Psi^N\rangle = NU/2|\Psi^N\rangle$ [50]. However, Yang's η-pairing state is no longer an eigenstate if one includes a nearest-neighbor interaction defined by

$$\mathcal{H}_V = \frac{V}{2}\sum_{\langle i,j\rangle} n_i n_j, \tag{45}$$

with $n_i = \sum_\sigma n_{i\sigma}$. As shown in Fig. 9(a), two doublons placed at adjacent sites gain additional energy of $4V$. Due to this, the interaction energy for each Fock state may change depending on the doublon configuration, which prevents Yang's η-pairing state from being an eigenstate of the Hubbard model with the nearest-neighbor interaction (Eq. (45)).

If we consider three-body interactions, on the other hand, we notice that an interaction between a doublon and a nearby particle can be used to cancel the nearest-neighbor two-body interaction (Eq. (45)), as shown in Fig. 9(b). In Yang's η-pairing state, the number of particles occupying each site is

equal to twice the number of doublons at the same site, since particles always exist as doublons. From this fact, one can see that Yang's η-pairing state satisfies

$$(\mathcal{H}_\mathrm{H} + \mathcal{H}_{\mathrm{mod}V})|\Psi^N\rangle = \frac{N}{2}U|\Psi^N\rangle, \tag{46}$$

$$\mathcal{H}_{\mathrm{mod}V} = \frac{V}{2}\sum_{\langle i,j\rangle} n_i(n_j - 2n_{j\uparrow}n_{j\downarrow}). \tag{47}$$

Therefore, utilizing the multi-body interaction, one can make Yang's η-pairing state an energy eigenstate even in the presence of the nearest-neighbor interaction (Eq. (45)).

We numerically confirm that Yang's η-pairing state can be regarded as a QMBS state in the model with the Hamiltonian $\mathcal{H}_\mathrm{H} + \mathcal{H}_{\mathrm{mod}V}$ in Eq. (46). For the half-filled one-dimensional system with the periodic boundary condition of length L, we numerically obtain the level-spacing distribution $P(s)$ (Fig. 9(c)) in the subspace with even parity, even time-reversal symmetry, and zero total momentum. The level-spacing distribution agrees well with the Winger–Dyson distribution $P_\mathrm{WD}(s)$, implying that the model ($\mathcal{H}_\mathrm{H} + \mathcal{H}_{\mathrm{mod}V}$) is nonintegrable. We also consider the corresponding model with the open boundary condition, for which the bipartite entanglement entropy for each energy eigenstate is shown in Fig. 9(d). We find that Yang's η-pairing state, indicated by the red circle, has much smaller entanglement entropy than the other thermal states (with $S_\mathrm{A} \gtrsim 3\ln 2$). Therefore, we conclude that Yang's η-pairing state is a nonthermal energy eigenstate (i.e., a QMBS state) in the multi-body interacting system with the Hamiltonian $\mathcal{H}_\mathrm{H} + \mathcal{H}_{\mathrm{mod}V}$.

D. p-wave η-pairing state in the one-dimensional spinless fermion system

Let us finally check that the p-wave η-pairing state discussed in Sec. II A also satisfies the conditions for a QMBS state in the extended spinless Hubbard model with the three-body interaction defined by Eq. (6). Figure 10(a) shows the level-spacing
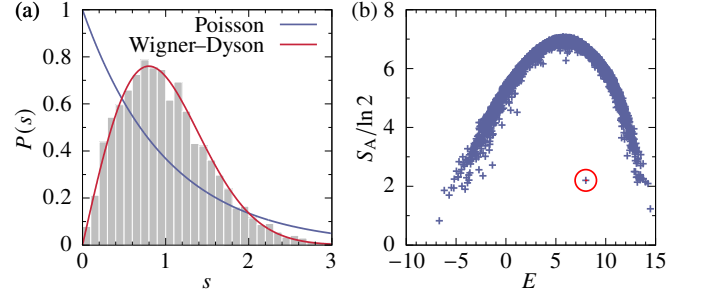

FIG. 10. (a) Nearset-neighbor level-spacing distribution $P(s)$ for the one-dimensional spinless Hubbard model with the three-body interaction (Eq. (6)) with $L = 20$. The blue and red curves correspond to the Poisson and Wigner-Dyson distribution, respectively. (b) Entanglement entropy spectrum of the energy eigenstates in the corresponding model with $L = 16$. The red circle indicates the p-wave η-pairing state (Eq. (2)). The parameters are set to be $t = 1$, $V = 2$, $W = -V/2$, $N = L/2$, and $\sigma_\mathrm{Gauss} = 0.5$.
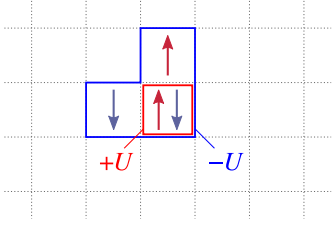
FIG. 11. Energy cancellation between the two-body on-site interaction (red box) and the multi-body interaction acting among a doublon and two neighboring particles (blue box).
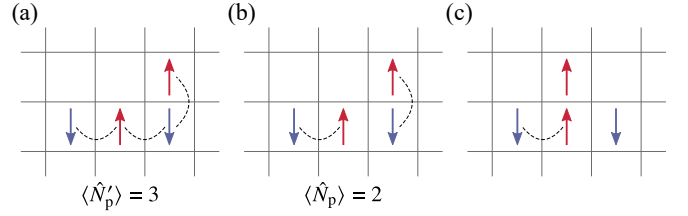

FIG. 12. Number of off-site pairs in examples of Fock states. (a) Expectation value of $\hat{N}'_\mathrm{p}$ in Eq. (49) for the case of two neighboring off-site pairs. (b) Expectation value of $\hat{N}_\mathrm{p}$ in Eq. (50) for the same state as in (a). (c) The case in which one pair is broken. The number of particles is given by $\langle \hat{N} \rangle/2 = 2$.

distribution $P(s)$ of the energy eigenstates on the half-filled periodic lattice in the subspace with odd parity and total momentum π. We observe good agreement between $P(s)$ and the Winger–Dyson distribution. Figure 10(b) shows the bipartite entanglement entropy spectrum in the open boundary chain at half filling. We find that the p-wave η-pairing state (Eq. (2)), indicated by the red circle, has much smaller entanglement entropy than those of the other eigenstates that form a convex upward curve. Therefore, the p-wave η-pairing state (Eq. (2)) can be regarded as a QMBS state in the multi-body interacting system (Eq. (6)).

VI. DISCUSSION

In this section, we discuss several aspects of the unconventional η-pairing states. In Sec. VI A, we show that the d-wave η-pairing state also becomes an eigenstate in a model with higher multi-body interaction. In Sec. VI B, we argue that the eigenenergy of the unconventional η-pairing states can be controlled by an effective chemical potential in terms of pair numbers.

A. Higher multi-body interactions

To achieve superconducting scar states, it is also possible to exploit higher multi-body interactions (i.e., M-body interactions with larger M). In the case of the d-wave η-pairing state on the square lattice (discussed in Sec. II), we find that a doublon created by an overlap between two pairs is always accompanied by two particles around the doublon. We can cancel the on-site two-body interaction with a multi-body interaction acting among a doublon and two associated particles, as shown by the blue box in Fig. 11. Motivated by this observation, we consider the following interaction term in the Hamiltonian,

$$\mathcal{H}'_\mathrm{int} = U \sum_i n_{i\uparrow} n_{i\downarrow} \left[1 - \mathbb{n}_{i\uparrow} \mathbb{n}_{i\downarrow} \right], \tag{48}$$

which contains up to $(2z + 2)$-body interactions. The d-wave η-pairing state is also an exact energy eigenstate of the model with the Hamiltonian $\mathcal{H}_\mathrm{kin} + \mathcal{H}'_\mathrm{int}$. Here we need to use the neighboring particle existence operator $\mathbb{n}_{i\sigma}$ (Eq. (17)) to cor-

rectly cancel the energy increment of overlapped pairs, as discussed in Sec. II D.

B. Pair number operator

The unconventional η-pairing states studied in this paper have high eigenenergies as compared to the ground-state energy. From a practical point of view, it will be convenient if we could control the eigenenergies of those pairing states. To this end, we introduce an operator that counts the number of pairs, extending the concept of the number operator for particles ($\hat{N} = \sum_{i\sigma} n_{i\sigma}$). Since off-site pairs considered in this paper are composed of two nearest-neighbor particles, one might think that the following operator could be used:

$$\hat{N}'_\mathrm{p} = \frac{1}{2} \sum_{\langle i,j \rangle \sigma} n_{i\sigma} n_{j\bar{\sigma}}, \tag{49}$$

with $\bar{\sigma} = \downarrow (\uparrow)$ for $\sigma = \uparrow (\downarrow)$. This operator is a part of the nearest-neighbor interaction in Eq. (45). However, as discussed in Sec. II C, the overcounting occurs when pairs are close to each other. Figure 12(a) shows one example of Fock states representing the d-wave η-pairing state. Although there are two pairs, the expectation value of $\hat{N}'_\mathrm{p}$ is 3. Indeed, the appropriate operator to count the number of pairs is given by

$$\hat{N}_\mathrm{p} = \frac{1}{2} \sum_{i\sigma} n_{i\sigma} \mathbb{n}_{i\bar{\sigma}}. \tag{50}$$

Using the neighboring particle existence operator $\mathbb{n}_{i\sigma}$ (Eq. (17)), we can measure the number of pairs correctly, as shown in Fig. 12(b). The η-pairing states become an eigenstate of $\hat{N}_p$:

$$\hat{N}_\mathrm{p} |\Psi^N_\alpha\rangle = \frac{N}{2} |\Psi^N_\alpha\rangle, \tag{51}$$

where $|\Psi^N_\alpha\rangle \propto (\eta^+_\alpha)^{N/2}|0\rangle$.

The operator $\hat{N}_\mathrm{p}$ is used to stabilize the unconventional η-pairing states over unpaired states. Figure 12(c) shows an example of a Fock state with one broken pair. The expectation value of $\hat{N}_\mathrm{p}$ for this state is 1.5. If we introduce a pair chemical potential μ_p and replace the Hamiltonian $\mathcal{H}_\mathrm{extH}$ with $\mathcal{H}_\mathrm{extH} - \mu_\mathrm{p}\hat{N}_\mathrm{p}$, we can decrease the eigenenergy of the unconventional pairing states than other unpaired eigenstates.

VII. SUMMARY

In this paper, we have presented a systematic framework to construct model Hamiltonians that have superconducting quantum many-body scar states with unconventional pairing symmetries (e.g., p-wave, d-wave, f-wave, etc.) by engineering multi-body interactions. The derived unconventional pairing states are natural extensions of Yang's s-wave η pairing states, and will be relevant for applications to nonthermal and long-lived nonequilibrium superconductivity with unconventional pairing symmetries. From the point of view of the renormalization principle [75], low-energy physics can be well described by few-body interactions in effective theories, which is not necessarily the case in high energies, where the multi-body interactions may play a role.

Finally, we briefly comment on possible experimental realizations of the multi-body interactions. In solid-state and cold-atom systems, one often considers a situation where particles are interacting via two-body interactions alone. However, it has been pointed out that multi-body interactions may arise in cuprate superconductors as a higher-order correction term coming from bands away from the Fermi energy [76]. Moreover, in cold-atom systems, a three-body interaction such as Eq. (8) has been realized as a controllable interactions [77–83]. Thus, cold-atom systems will be a suitable playground to realize the superconducting scar states, especially for those composed of spinless fermions discussed in Secs. II A and V D.

[1] D. Fausti, R. I. Tobey, N. Dean, S. Kaiser, A. Dienst, M. C. Hoffmann, S. Pyon, T. Takayama, H. Takagi, and A. Cavalleri, Light-induced superconductivity in a stripe-ordered cuprate, Science 331, 189 (2011).

[2] S. Kaiser, C. R. Hunt, D. Nicoletti, W. Hu, I. Gierz, H. Y. Liu, M. Le Tacon, T. Loew, D. Haug, B. Keimer, and A. Cavalleri, Optically induced coherent transport far above T_c in underdoped YBa$_2$Cu$_3$O$_{6+\delta}$, Phys. Rev. B 89, 184516 (2014).

[3] W. Hu, S. Kaiser, D. Nicoletti, C. R. Hunt, I. Gierz, M. C. Hoffmann, M. Le Tacon, T. Loew, B. Keimer, and A. Cavalleri, Optically enhanced coherent transport in YBa$_2$Cu$_3$O$_{6.5}$ by ultrafast redistribution of interlayer coupling, Nat. Mater. 13, 705 (2014).

[4] M. Mitrano, A. Cantaluppi, D. Nicoletti, S. Kaiser, A. Perucchi, S. Lupi, P. Di Pietro, D. Pontiroli, M. Riccò, S. R. Clark, D. Jaksch, and A. Cavalleri, Possible light-induced superconductivity in K$_3$C$_{60}$ at high temperature, Nature 530, 461 (2016).

[5] K. A. Cremin, J. Zhang, C. C. Homes, G. D. Gu, Z. Sun, M. M. Fogler, A. J. Millis, D. N. Basov, and R. D. Averitt, Photoenhanced metastable c-axis electrodynamics in stripe-ordered cuprate La$_{1.885}$Ba$_{0.115}$CuO$_4$, Proc. Natl. Acad. Sci. 116, 19875 (2019).

[6] K. Katsumi, M. Nishida, S. Kaiser, S. Miyasaka, S. Tajima, and R. Shimano, Near-infrared light-induced superconducting-like state in underdoped YBa$_2$Cu$_3$O$_y$ studied by c-axis terahertz third-harmonic generation, Phys. Rev. B 107, 214506 (2023).

[7] S. J. Zhang, X. Y. Zhou, S. X. Xu, Q. Wu, L. Yue, Q. M. Liu, T. C. Hu, R. S. Li, J. Y. Yuan, C. C. Homes, G. D. Gu, T. Dong, and N. L. Wang, Light-Induced Melting of Competing Stripe Orders without Introducing Superconductivity in La$_{2-x}$Ba$_x$CuO$_4$, Phys. Rev. X 14, 011036 (2024).

[8] L. D. Marin Bukov and A. Polkovnikov, Universal high-frequency behavior of periodically driven systems: from dynamical stabilization to Floquet engineering, Adv. Phys. 64, 139 (2015).

[9] T. Oka and S. Kitamura, Floquet Engineering of Quantum Materials, Annu. Rev. Condens. Matter Phys. 10, 387 (2019).

[10] N. Tsuji, Floquet states, in Encyclopedia of Condensed Matter Physics (Second Edition), edited by T. Chakraborty (Academic Press, Oxford, 2024) second edition ed., pp. 967–980.

[11] M. Ezawa, Photo-Induced Topological Superconductor in Silicene, Germanene, and Stanene, J. Supercond. Nov. Magn. 28, 1249 (2015).

[12] K. Takasan, A. Daido, N. Kawakami, and Y. Yanase, Laser-induced topological superconductivity in cuprate thin films, Phys. Rev. B 95, 134508 (2017).

[13] H. Chono, K. Takasan, and Y. Yanase, Laser-induced topological s-wave superconductivity in bilayer transition metal dichalcogenides, Phys. Rev. B 102, 174508 (2020).

[14] P. Wenk, M. Grifoni, and J. Schliemann, Topological transitions in two-dimensional Floquet superconductors, Phys. Rev. B 106, 134508 (2022).

[15] Y. Yanase, A. Daido, K. Takasan, and T. Yoshida, Topological d-wave superconductivity in two dimensions, Phys. E: Low-Dimens. Syst. Nanostructures 140, 115143 (2022).

[16] S. Kitamura and H. Aoki, Floquet topological superconductivity induced by chiral many-body interaction, Commun. Phys. 5, 174 (2022).

[17] J. Cayao, C. Triola, and A. M. Black-Schaffer, Floquet engineering bulk odd-frequency superconducting pairs, Phys. Rev. B 103, 104505 (2021).

[18] J. Cayao and A. M. Black-Schaffer, Exceptional odd-frequency pairing in non-Hermitian superconducting systems, Phys. Rev. B 105, 094502 (2022).

[19] T. Kaneko, T. Shirakawa, S. Sorella, and S. Yunoki, Photo-induced η Pairing in the Hubbard Model, Phys. Rev. Lett. 122, 077002 (2019).

[20] M. Malakhov and M. Avdeev, Non-equilibrium d-wave pair density wave order parameter in superconducting cuprates, Phys. C: Supercond. its Appl. 581, 1353820 (2021).

[21] H. Bernien, S. Schwartz, A. Keesling, H. Levine, A. Omran, H. Pichler, S. Choi, A. S. Zibrov, M. Endres, M. Greiner, V. Vuletić, and M. D. Lukin, Probing many-body dynamics on a 51-atom quantum simulator, Nature 551, 579 (2017).

[22] N. Shiraishi and T. Mori, Systematic Construction of Counterexamples to the Eigenstate Thermalization Hypothesis, Phys. Rev. Lett. 119, 030601 (2017).

[23] C. J. Turner, A. A. Michailidis, D. A. Abanin, M. Serbyn, and Z. Papić, Weak ergodicity breaking from quantum many-body scars, Nat. Phys. 14, 745 (2018).

[24] J. M. Deutsch, Quantum statistical mechanics in a closed system, Phys. Rev. A **43**, 2046 (1991).

[25] M. Srednicki, Chaos and quantum thermalization, Phys. Rev. E **50**, 888 (1994).

[26] M. Rigol, V. Dunjko, and M. Olshanii, Thermalization and its mechanism for generic isolated quantum systems, Nature **452**, 854 (2008).

[27] J. M. Deutsch, Eigenstate thermalization hypothesis, Rep. Prog. Phys. **81**, 082001 (2018).

[28] M. Serbyn, D. A. Abanin, and Z. Papić, Quantum many-body scars and weak breaking of ergodicity, Nat. Phys. **17**, 675 (2021).

[29] Z. Papić, Weak Ergodicity Breaking Through the Lens of Quantum Entanglement, in *Entanglement in Spin Chains: From Theory to Quantum Technology Applications*, edited by A. Bayat, S. Bose, and H. Johannesson (Springer, Cham, 2022) pp. 341–395.

[30] S. Moudgalya, B. A. Bernevig, and N. Regnault, Quantum many-body scars and Hilbert space fragmentation: a review of exact results, Rep. Prog. Phys. **85**, 086501 (2022).

[31] A. Chandran, T. Iadecola, V. Khemani, and R. Moessner, Quantum Many-Body Scars: A Quasiparticle Perspective, Annu. Rev. Condens. Matter Phys. **14**, 443 (2023).

[32] S. Moudgalya, N. Regnault, and B. A. Bernevig, Entanglement of exact excited states of Affleck-Kennedy-Lieb-Tasaki models: Exact results, many-body scars, and violation of the strong eigenstate thermalization hypothesis, Phys. Rev. B **98**, 235156 (2018).

[33] M. Schecter and T. Iadecola, Weak Ergodicity Breaking and Quantum Many-Body Scars in Spin-1 *XY* Magnets, Phys. Rev. Lett. **123**, 147201 (2019).

[34] S. Pai and M. Pretko, Dynamical Scar States in Driven Fracton Systems, Phys. Rev. Lett. **123**, 136401 (2019).

[35] J. Ren, C. Liang, and C. Fang, Quasisymmetry Groups and Many-Body Scar Dynamics, Phys. Rev. Lett. **126**, 120604 (2021).

[36] X. Yu, D. Luo, and B. K. Clark, Beyond many-body localized states in a spin-disordered Hubbard model, Phys. Rev. B **98**, 115106 (2018).

[37] S. Scherg, T. Kohlert, P. Sala, F. Pollmann, B. Hebbe Madhusudhana, I. Bloch, and M. Aidelsburger, Observing non-ergodicity due to kinetic constraints in tilted Fermi-Hubbard chains, Nat. Commun. **12**, 4490 (2021).

[38] S. Chattopadhyay, H. Pichler, M. D. Lukin, and W. W. Ho, Quantum many-body scars from virtual entangled pairs, Phys. Rev. B **101**, 174308 (2020).

[39] C.-J. Lin, V. Calvera, and T. H. Hsieh, Quantum many-body scar states in two-dimensional Rydberg atom arrays, Phys. Rev. B **101**, 220304 (2020).

[40] Y. Kuno, T. Mizoguchi, and Y. Hatsugai, Flat band quantum scar, Phys. Rev. B **102**, 241115 (2020).

[41] S. Sugiura, T. Kuwahara, and K. Saito, Many-body scar state intrinsic to periodically driven system, Phys. Rev. Res. **3**, L012010 (2021).

[42] P. Zhang, H. Dong, Y. Gao, L. Zhao, J. Hao, J.-Y. Desaules, Q. Guo, J. Chen, J. Deng, B. Liu, W. Ren, Y. Yao, X. Zhang, S. Xu, K. Wang, F. Jin, X. Zhu, B. Zhang, H. Li, C. Song, Z. Wang, F. Liu, Z. Papić, L. Ying, H. Wang, and Y.-C. Lai, Many-body Hilbert space scarring on a superconducting processor, Nat. Phys. **19**, 120 (2023).

[43] G.-X. Su, H. Sun, A. Hudomal, J.-Y. Desaules, Z.-Y. Zhou, B. Yang, J. C. Halimeh, Z.-S. Yuan, Z. Papić, and J.-W. Pan, Observation of many-body scarring in a Bose-Hubbard quantum simulator, Phys. Rev. Res. **5**, 023010 (2023).

[44] K. Omiya and M. Müller, Quantum many-body scars in bipartite Rydberg arrays originating from hidden projector embedding, Phys. Rev. A **107**, 023318 (2023).

[45] K. Omiya and M. Müller, Fractionalization paves the way to local projector embeddings of quantum many-body scars, Phys. Rev. B **108**, 054412 (2023).

[46] J.-Y. Desaules, A. Hudomal, C. J. Turner, and Z. Papić, Proposal for Realizing Quantum Scars in the Tilted 1D Fermi-Hubbard Model, Phys. Rev. Lett. **126**, 210601 (2021).

[47] R. Kaneko, M. Kunimi, and I. Danshita, Quantum many-body scars in the Bose-Hubbard model with a three-body constraint, Phys. Rev. A **109**, L011301 (2024).

[48] C. Matsui, Exactly solvable subspaces of nonintegrable spin chains with boundaries and quasiparticle interactions, Phys. Rev. B **109**, 104307 (2024).

[49] K. Pakrouski, P. N. Pallegar, F. K. Popov, and I. R. Klebanov, Many-Body Scars as a Group Invariant Sector of Hilbert Space, Phys. Rev. Lett. **125**, 230602 (2020).

[50] C. N. Yang, η pairing and off-diagonal long-range order in a Hubbard model, Phys. Rev. Lett. **63**, 2144 (1989).

[51] C. N. Yang and S. Zhang, SO$_4$ SYMMETRY IN A HUBBARD MODEL, Mod. Phys. Lett. B **04**, 759 (1990).

[52] O. Vafek, N. Regnault, and B. A. Bernevig, Entanglement of exact excited eigenstates of the Hubbard model in arbitrary dimension, SciPost Phys. **3**, 043 (2017).

[53] K. Li, η-pairing in correlated fermion models with spin-orbit coupling, Phys. Rev. B **102**, 165150 (2020).

[54] D. K. Mark and O. I. Motrunich, η-pairing states as true scars in an extended Hubbard model, Phys. Rev. B **102**, 075132 (2020).

[55] S. Moudgalya, N. Regnault, and B. A. Bernevig, η-pairing in Hubbard models: From spectrum generating algebras to quantum many-body scars, Phys. Rev. B **102**, 085140 (2020).

[56] K. Pakrouski, P. N. Pallegar, F. K. Popov, and I. R. Klebanov, Group theoretic approach to many-body scar states in fermionic lattice models, Phys. Rev. Res. **3**, 043156 (2021).

[57] J. Wildeboer, C. M. Langlett, Z.-C. Yang, A. V. Gorshkov, T. Iadecola, and S. Xu, Quantum many-body scars from Einstein-Podolsky-Rosen states in bilayer systems, Phys. Rev. B **106**, 205142 (2022).

[58] Z. Sun, F. K. Popov, I. R. Klebanov, and K. Pakrouski, Majorana scars as group singlets, Phys. Rev. Res. **5**, 043208 (2023).

[59] P. Kolb and K. Pakrouski, Stability of the Many-Body Scars in Fermionic Spin-1/2 Models, PRX Quantum **4**, 040348 (2023).

[60] S. Hoshino, Mean-field description of odd-frequency superconductivity with staggered ordering vector, Phys. Rev. B **90**, 115154 (2014).

[61] N. Tsuji, M. Nakagawa, and M. Ueda, Tachyonic and Plasma Instabilities of η-Pairing States Coupled to Electromagnetic Fields, arXiv:2103.01547.

[62] K. Tamura and H. Katsura, Quantum many-body scars of spinless fermions with density-assisted hopping in higher dimensions, Phys. Rev. B **106**, 144306 (2022).

[63] L. Gotta, L. Mazza, P. Simon, and G. Roux, Exact many-body scars based on pairs or multimers in a chain of spinless fermions, Phys. Rev. B **106**, 235147 (2022).

[64] H. Zhai, Two generalizations of η pairing in extended Hubbard models, Phys. Rev. B **71**, 012512 (2005).

[65] M. Nakagawa, H. Katsura, and M. Ueda, Exact eigenstates of multicomponent Hubbard models: SU(N) magnetic η pairing, weak ergodicity breaking, and partial integrability, arXiv:2205.07235.

[66] H. Yoshida and H. Katsura, Exact eigenstates of extended SU(N) Hubbard models: Generalization of η-pairing states with N-particle off-diagonal long-range order, Phys. Rev. B **105**, 024520 (2022).

[67] S. Ray, Y. Murakami, and P. Werner, Nonthermal superconductivity in photodoped multiorbital Hubbard systems, Phys. Rev. B **108**, 174515 (2023).

[68] A. Y. Kitaev, Unpaired Majorana fermions in quantum wires, Phys.-Usp. **44**, 131 (2001).

[69] The spin-singlet state is defined as $\left(c_{a\uparrow}^{\dagger} c_{b\downarrow}^{\dagger} - c_{a\downarrow}^{\dagger} c_{b\uparrow}^{\dagger} \right) |0\rangle$, where $c_{\xi\sigma}$ is the annihilation operator with spin σ and the other quantum number ξ ($= a, b$). For the η-pairing states, the quantum number ξ corresponds to spatial positions, for example, $a = \boldsymbol{r}_i$ and $b = \boldsymbol{r}_i + \boldsymbol{e}_x$. Referring to this definition, we obtain the spin-singlet η-pairing operator as $\eta_{+\boldsymbol{e}_x}^{+} - \eta_{-\boldsymbol{e}_x}^{+}$.

[70] E. Bianchi, L. Hackl, M. Kieburg, M. Rigol, and L. Vidmar, Volume-Law Entanglement Entropy of Typical Pure Quantum States, PRX Quantum **3**, 030201 (2022).

[71] D. N. Page, Average entropy of a subsystem, Phys. Rev. Lett. **71**, 1291 (1993).

[72] The d-wave η-pairing state is the eignestate in the $\mathcal{P}_x \mathcal{P}_y = 1$ subspace, but not an eigenstate in each of the $\mathcal{P}_x$ and $\mathcal{P}_y$ eigenspaces. In each space, the d-wave η-pairing state is degenerate with the s-wave η-pairing state described in Sec. V A, since both η-pairing operators satisfy the relation $\mathcal{P}_x \eta_d^{+} \mathcal{P}_x = \eta_s^{+}$, for example.

[73] H. Bruus and J.-C. Angl'es d'Auriac, Energy level statistics of the two-dimensional Hubbard model at low filling, Phys. Rev. B **55**, 9142 (1997).

[74] J. M. G. Gómez, R. A. Molina, A. Relaño, and J. Retamosa, Mis-

leading signatures of quantum chaos, Phys. Rev. E **66**, 036209 (2002).

[75] S. Weinberg, Phenomenological Lagrangians, Phys. A Stat. Mech. its Appl. **96**, 327 (1979).

[76] M. E. Simón, A. A. Aligia, and E. R. Gagliano, Optical properties of an effective one-band Hubbard model for the cuprates, Phys. Rev. B **56**, 5637 (1997).

[77] H. P. Büchler, A. Micheli, and P. Zoller, Three-body interactions with cold polar molecules, Nat. Phys. **3**, 726 (2007).

[78] J. Han, Direct evidence of three-body interactions in a cold ^{85}Rb Rydberg gas, Phys. Rev. A **82**, 052501 (2010).

[79] S. Will, T. Best, U. Schneider, L. Hackermüller, D.-S. Lühmann, and I. Bloch, Time-resolved observation of coherent multi-body interactions in quantum phase revivals, Nature **465**, 197 (2010).

[80] H.-W. Hammer, A. Nogga, and A. Schwenk, Colloquium : Three-body forces: From cold atoms to nuclei, Rev. Mod. Phys. **85**, 197 (2013).

[81] J. Ren, Y.-Z. Wu, and X.-F. Xu, Expansion dynamics in a one-dimensional hard-core boson model with three-body interactions, Sci. Rep. **5**, 14743 (2015).

[82] M. Valiente, Three-body repulsive forces among identical bosons in one dimension, Phys. Rev. A **100**, 013614 (2019).

[83] K. Honda, Y. Takasu, Y. Haruna, Y. Nishida, and Y. Takahashi, Evidence of a Four-Body Force in an Interaction-Tunable Trapped Cold-Atom System, arXiv:2402.16254.